AGU PUBLICATIONS

Global Biogeochemical Cycles

RESEARCH ARTICLE
10.1002/2015GB005110

Key Points:
- CO_2 undersaturation in the Amazon River plume supported by biological activity
- The area is a net sink of atmospheric CO_2
- Positive temperature anomalies led to CO_2 outgassing in the NEC in 2010

Correspondence to:
J. S. P. Ibánhez,
pinoibaj@tcd.ie

Citation:
Ibánhez, J. S. P., D. Diverrès, M. Araujo, and N. Lefèvre (2015), Seasonal and interannual variability of sea-air CO_2 fluxes in the tropical Atlantic affected by the Amazon River plume, *Global Biogeochem. Cycles*, *29*, 1640–1655, doi:10.1002/2015GB005110.

Received 4 FEB 2015
Accepted 5 SEP 2015
Accepted article online 9 SEP 2015
Published online 5 OCT 2015

Seasonal and interannual variability of sea-air CO_2 fluxes in the tropical Atlantic affected by the Amazon River plume

J. Severino P. Ibánhez[1,2], Denis Diverrès[3], Moacyr Araujo[2], and Nathalie Lefèvre[2,4]

[1]Institut de Recherche pour le Développement, Brasília-DF, Brazil, [2]Department of Oceanography, Center for Risk Analysis and Environmental Modeling, Federal University of Pernambuco, Recife PE, Brazil, [3]US 191, Centre IRD de Bretagne, BP 70, Plouzané, France, [4]IRD-LOCEAN, Sorbonne Universités (Université Pierre et Marie Curie-CNRS-MNHN), Paris, France

Abstract CO_2 fugacities obtained from a merchant ship sailing from France to French Guyana were used to explore the seasonal and interannual variability of the sea-air CO_2 exchange in the western tropical North Atlantic (TNA; 5–14°N, 41–52°W). Two distinct oceanic water masses were identified in the area associated to the main surface currents, i.e., the North Brazil Current (NBC) and the North Equatorial Current (NEC). The NBC was characterized by permanent CO_2 oversaturation throughout the studied period, contrasting with the seasonal pattern identified in the NEC. The NBC retroflection was the main contributor to the North Equatorial Counter Current (NECC), thus spreading into the central TNA, the Amazon River plume, and the CO_2-rich waters probably originated from the equatorial upwelling. Strong CO_2 undersaturation was associated to the Amazon River plume. Total inorganic carbon drawdown due to biological activity was estimated to be 154 μmol kg^{-1} within the river plume. As a consequence, the studied area acted as a net sink of atmospheric CO_2 (from -72.2 ± 10.2 mmol m^{-2} $month^{-1}$ in February to 14.3 ± 4.5 mmol m^{-2} $month^{-1}$ in May). This contrasted with the net CO_2 efflux estimated by the main global sea-air CO_2 flux climatologies. Interannual sea surface temperature changes in the TNA caused by large-scale climatic events could determine the direction and intensity of the sea-air CO_2 fluxes in the NEC. Positive temperature anomalies observed in the TNA led to an almost permanent CO_2 outgassing in the NEC in 2010.

1. Introduction

The tropical Atlantic is one of the largest oceanic sources of CO_2 to the atmosphere. Recent global sea-air CO_2 flux climatologies estimated that this region is the second largest oceanic source of CO_2 to the atmosphere after the tropical Pacific [*Takahashi et al.*, 2009; *Landschützer et al.*, 2014], with a consistent mean sea-air CO_2 flux between 0.11 Pg C y^{-1} (year 2000) [*Takahashi et al.*, 2009] and 0.10 ± 0.06 Pg C y^{-1} (year 2010) [*Landschützer et al.*, 2014], estimated in the 18°S–18°N latitudinal band. The zonal spread of CO_2-rich waters originated from the equatorial upwelling system and transported westward by the South Equatorial Current (SEC) explains this permanent net CO_2 outgassing [e.g., *Andrié et al.*, 1986]. However, strong latitudinal gradients of the fugacity of CO_2 (fCO_2) in the tropical Atlantic appear associated to the main surface water circulation [*Lefèvre et al.*, 2014]. Zonal current bands in the tropical Atlantic coexist with the meridional overturning circulation, which determines a net northward transport of water and heat [*Stramma and Schott*, 1999; *Kirchner et al.*, 2009]. The complex sea surface circulation in the tropical Atlantic determines the interhemispheric exchange of water with different origins and physical and chemical properties. Nevertheless, studies on the influence of the surface water circulation over the sea-air CO_2 exchange in the tropical Atlantic are rare to date [e.g.. *Lefèvre et al.*, 2014].

Despite that the tropical Atlantic is regarded as a net source of CO_2 to the atmosphere, CO_2 undersaturation areas exist due to precipitation or riverine influence. The Amazon River is the largest river in the world in terms of freshwater discharge to the oceans [e.g., *Chen et al.*, 2012]. As it discharges to the western tropical North Atlantic (hereafter TNA), the Amazon River develops a plume that can exceed 10^6 km^2, covering a vast portion of the western tropical Atlantic and reaching latitudes as far as 30°W [*Coles et al.*, 2013]. The upper Amazon River is a net source of CO_2 to the atmosphere largely fueled by CO_2 and organic matter exportation from flooded wetlands and organic matter mineralization along the river path [*Abril et al.*, 2014]. When it mixes with oceanic waters, the Amazon River plume becomes a significant atmospheric CO_2 sink [*Ternon et al.*, 2000;

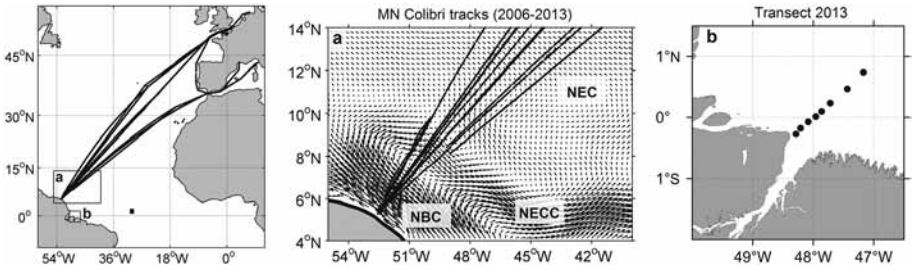

Figure 1. Tracks of the *MN Colibri*, the transect perpendicular to the Amazon River mouth and the location of the sampling station of the Camadas Finas 2 cruise (black square) used in this study. (a) Details of the studied area, along with the surface velocity climatology for the month of October (computed for the period 1992–2012). The main surface currents are indicated: the North Brazil Current (NBC), the North Equatorial Countercurrent (NECC), and the North Equatorial Current (NEC). (b) Location of the sampling stations in the transect perpendicular to the Amazon River mouth.

Körtzinger, 2003; *Cooley et al*., 2007; *Lefèvre et al*., 2010]. *Körtzinger* [2003] estimated that the Amazon River plume would be responsible for a carbon sink of 0.014 ± 0.005 Pg C yr^{-1}, a similar value to that reported by *Cooley et al*. [2007] for the outer plume sink (0.015 ± 0.006 Pg C yr^{-1}), and higher than that calculated by *Lefèvre et al*. [2010] (0.005 Pg C yr^{-1}), who considered a smaller River plume area. Thus, the Amazon River plume could be responsible for an atmospheric CO_2 sink that could roughly represent 10% of the estimated CO_2 outgassing associated to the tropical Atlantic.

The contribution of the different factors explaining the CO_2 undersaturation of the Amazon River plume and its seasonal variability is not clear. *Ternon et al*. [2000] estimated that primary production within the plume would be responsible for about 30% of the observed CO_2 undersaturation. On the other hand, *Cooley et al*. [2007] suggested that net primary production in the River plume would enhance the observed CO_2 undersaturation by a hundredfold. Elucidation of the physical and biological processes responsible for the modulation of the fCO_2 in the Amazon River plume and the western TNA may help in better constraining the role of the tropical Atlantic in the global sea-air CO_2 exchange. Furthermore, the impact of interannual, large-scale climatic events, which has been shown to strongly determine the sea-air CO_2 exchange in the eastern tropical Atlantic [*Lefèvre et al*., 2013], is currently unknown for the area. This information is crucial to understand how the tropical Atlantic would react to the current and projected environmental changes such as atmospheric CO_2 increase or sea surface temperature (SST) changes.

Here we present a high spatial and temporal resolution CO_2 fugacity (fCO_2) data set obtained from a ship of opportunity (*MN Colibri*) that has performed continuous measurements in the surface waters of the western TNA since 2006. A total of 30 voyages of the *MN Colibri* have been made, allowing to obtain an almost complete picture of the seasonality of the fCO_2 in the area affected by the Amazon River plume. The objective of this study is to determine the main seasonal and interannual drivers of the sea-air CO_2 exchange variability in the oceanic area affected by the Amazon River plume.

2. Methods

An automated CO_2 analyzer similar to that described by *Pierrot et al*. [2009] was installed on board the merchant ship *MN Colibri* sailing from Le Havre (mainland France) to Kourou (French Guyana) in 2006. The ship was also equipped with a Seabird thermosalinograph and a Druck barometer for continuous SST, sea surface salinity (SSS), and atmospheric pressure (*P*) measurements. Data collected between 14°N and Kourou (5°12′N, 52°46′W) were used to explore sea-air CO_2 fluxes along the *MN Colibri* tracks under the influence of the Amazon River plume (Figure 1). A total of 30 voyages recorded data in the selected region (Table 1). The *MN Colibri* did not follow the same route throughout the study period (Figure 1; see Table 1 for details on the individual routes followed by the *MN Colibri*). Instead, the maximum longitudinal difference among the *MN Colibri* tracks at the northernmost limit of the studied area was 7° (from 45 to 52°W, Table 1).

Measurements of the atmospheric molar fraction of CO_2, xCO_{2atm}, made on board the *MN Colibri* during cruises 1 to 7, 10, 12, 15, 23, 24, 26, and 29 (Table 1) were contaminated by the flumes of the ship. In these cases, the monthly xCO_{2atm} recorded at the closest atmospheric station of the NOAA/Earth System Research Laboratory

Table 1. Voyages of the *MN Colibri* Used in This Study[a]

Number	Dates of the Voyages	Minimum Latitude	Maximum Latitude	Minimum Longitude	Maximum Longitude	Route	Representative Month
1	4–6 March 2006	5°N	14°N	45°W	52°W	Le Havre-Kourou	March
2	8–10 March 2006	5°N	14°N	47°W	52°W	Kourou-Le Havre	March
3	28–30 April 2007	5°N	14°N	42°W	51°W	Le Havre-Kourou	April
4	7–8 May 2007	9°N	14°N	42°W	47°W	Kourou-Le Havre	May
5	21–23 June 2007	5°N	14°N	44°W	52°W	Le Havre-Kourou	June
6	24–26 August 2007	5°N	14°N	45°W	52°W	Le Havre-Kourou	August
7	3–5 July 2008	5°N	14°N	45°W	52°W	Le Havre-Kourou	July
8	1–3 March 2009	5°N	14°N	44°W	52°W	Le Havre-Kourou	March
9	7–9 March 2009	5°N	14°N	46°W	52°W	Kourou-Le Havre	March
10	10–11 July 2009	10°N	14°N	41°W	45°W	Kourou-Le Havre	July
11	16–18 August 2009	5°N	14°N	45°W	52°W	Le Havre-Kourou	August
12	26–28 August 2009	5°N	14°N	46°W	52°W	Kourou-Le Havre	August
13	3–5 April 2010	6°N	14°N	45°W	51°W	Le Havre-Kourou	April
14	11–13 April 2010	8°N	14°N	41°W	48°W	Kourou-Le Havre	April
15	21–24 May 2010	5°N	14°N	44°W	52°W	Le Havre-Kourou	May
16	19–22 June 2010	8°N	14°N	41°W	48°W	Kourou-Le Havre	June
17	7–8 August 2010	7°N	14°N	45°W	51°W	Le Havre-Kourou	August
18	9–10 October 2010	11°N	14°N	43°W	46°W	Le Havre-Kourou	October
19	18–19 October 2010	10°N	14°N	44°W	48°W	Kourou-Le Havre	October
20	31 December 2010 to 2 January 2011	5°N	14°N	44°W	52°W	Le Havre-Kourou	December
21	7–8 January 2011	6°N	14°N	46°W	51°W	Kourou-Le Havre	January
22	16–17 June 2011	5°N	14°N	45°W	52°W	Le Havre-Kourou	June
23	29–31 January 2012	6°N	14°N	44°W	51°W	Le Havre-Kourou	January
24	17–19 March 2012	5°N	14°N	45°W	52°W	Le Havre-Kourou	March
25	22–24 March 2012	8°N	14°N	42°W	49°W	Kourou-Le Havre	March
26	30 November to 1 December 2012	5°N	14°N	46°W	52°W	Le Havre-Kourou	November
27	5–7 December 2012	7°N	14°N	45°W	51°W	Kourou-Le Havre	December
28	27–29 January 2013	5°N	14°N	45°W	52°W	Le Havre-Kourou	January
29	1–3 February 2013	6°N	14°N	45°W	51°W	Kourou-Le Havre	February
30	17-19 July 2013	5°N	14°N	45°W	52°W	Le Havre-Kourou	July

[a]The limits of the ship tracks used here and the dates the ship performed each track are also shown.

(ESRL) Global Monitoring Division (Ragged Point, Barbados, 13.17°N, 59.43°W; http://www.esrl.noaa.gov/gmd/ccgg/iadv/) was used. Atmospheric fCO_2 (fCO_{2atm}) was calculated from xCO_{2atm} according to

$$fCO_{2atm} = xCO_{2atm}(P - pH_2O)C_f \quad (1)$$

where pH_2O is the water vapor pressure at 100% humidity calculated from the measured SST and SSS and C_f is the fugacity coefficient calculated according to *Weiss* [1974]. Cruises 4, 8, and 9 lacked atmospheric pressure measurements due to a malfunctioning of the barometer. For these three cruises, the monthly atmospheric pressure obtained from the National Centers for Environmental Prediction (NCEP)/National Center for Atmospheric Research reanalysis project was used for the subsequent fCO_{2atm} calculation from xCO_{2atm}. For comparison, fCO_{2atm} derived from Ragged Point was also calculated for the voyages where xCO_{2atm} was measured. Good agreement between the fCO_{2atm} derived from the measured xCO_{2atm} and that calculated at the Ragged Point station was obtained, with a close to 1:1 relationship (Colibri $fCO_{2atm} = 6.1 + 0.99$ Barbados fCO_{2atm}; $R = 0.94$; $n = 16$; $p < 0.0001$).

Sea-air CO_2 fluxes (F) along the tracks of the *MN Colibri* were calculated according to

$$F = k\, S_o(fCO_{2sw} - fCO_{2atm}) \quad (2)$$

where S_o is the solubility of CO_2 as a function of SST and SSS [*Weiss*, 1974], k is the gas transfer velocity and fCO_{2sw} is the fCO_2 of the surface ocean waters. Gas transfer velocity (k) was calculated according to *Sweeney et al.* [2007]:

$$k = 0.27\, U_{10}^2 (Sc/660)^{-0,5} \quad (3)$$

where Sc is the Schmidt number and U_{10} the wind speed at 10 m above sea level. U_{10} was obtained from the European Centre for Medium-Range Weather Forecasts reanalysis data set (ERA-interim). Monthly-averaged wind fields were interpolated at each position of the *MN Colibri* where measurements were taken (SST, SSS, P, and fCO_2).

Monthly mean, zonal surface water velocities (0.5 m depth) and SST were obtained from the Mercator Ocean GLORYS2V3 global ocean reanalysis with a 0.25° resolution. The downloaded surface water velocity grid was interpolated at each location of the *MN Colibri* where measurements were performed. Additionally, the Mercator monthly mean results for the period from 1992 to 2012 were used to compute climatological monthly surface water velocities (Figure 1a) and SST. SST anomalies were then computed by comparing the measured SST with the calculated climatological SST derived from the Mercator data.

Monthly Amazon River discharge was obtained from the Environmental Research Observatory HYBAM (geodynamical, hydrological, and biogeochemical control of erosion/alteration and material transport in the Amazon basin, http://www.ore-hybam.org). The values recorded at the Óbidos gauging station for the period 1992–2013 were used to calculate the climatological river discharge. Discharge anomalies were then computed for the period covered in this study (2006–2013). Satellite-derived, monthly-averaged chlorophyll *a* concentration was obtained from the Moderate Resolution Imaging Spectroradiometer (MODIS)/Aqua satellite with a 4 km resolution and processed with the OC3M algorithm and standard NASA global coefficients [*O'Reilly et al*., 1998].

Seawater samples for total inorganic carbon (TCO_2) and alkalinity (TA) analyses were taken during the Camadas Finas 2 cruise performed in October 2012 and a transect performed perpendicular to the eastern Amazon River mouth during April 2013 (Figure 1b). TCO_2 and TA were measured by potentiometric titration using a closed cell, following the method of *Edmond* [1970]. Equivalent points were calculated using the code published by *Department of Energy* [1994]. Certified Reference Material, supplied by Professor A. Dickson (Scripps Institutions of Oceanography, San Diego, USA), was used for calibration. The accuracy was estimated at 3 $\mu mol\,kg^{-1}$.

3. Results and Discussion

3.1. Distribution of SST, SSS, and fCO_{2sw} Along the *MN Colibri* Tracks

Almost all the cruises of the *MN Colibri* used here showed minimum salinities lower than 35 practical salinity unit (psu) within the studied area (Figure 2), with values ranging from 36.6 to 17.3 psu. Steep latitudinal SST gradients appeared closely related to SSS gradients, where the transition from oceanic to brackish waters was characterized by an increase in SST. The spatial extent of the influence of brackish waters was highly variable. From January to March, salinities lower than 35 psu were generally observed south of 8°N. From April to December, brackish waters were detected progressively farther north, reaching 12.58°N in December (Figure 2). In July–August, the retroflection of the North Brazilian Current (NBC) starts and transports the Amazon River plume to the northeast, joining the North Equatorial Countercurrent (NECC, Figure 1). From August to December, the presence of two separated SSS minima along the *MN Colibri* tracks (only one SSS minimum was observed in October due to the lack of data south of 10°N) clearly shows the influence of the local surface water circulation on the spread of Amazon waters in the TNA.

fCO_{2sw} along the tracks of the *MN Colibri* was highly variable, ranging from 122.9 to 438 μatm. fCO_{2sw} showed a strong relationship with SSS consistent with previous studies (Figure 3) [*Ternon et al*., 2000; *Körtzinger*, 2003; *Lefèvre et al*., 2010]. A significant linear relationship of fCO_{2sw} and SSS was obtained in our entire data set ($R = 0.83$, $p < 0.0001$, and $n = 27689$). Nevertheless, for comparison with previous studies, the linear relationship between fCO_{2sw} and SSS was calculated using the data associated to salinities lower than 35 psu (Figure 3). The following relationship was obtained:

$$fCO_{2sw} = 15.5(\pm 0.1)SSS - 159(\pm 3)(R = 0.9; n = 6393), \text{standard error of estimate} \pm 23.5\ \mu atm \quad (4)$$

Lefèvre et al. [2010] obtained a very similar linear relationship of fCO_{2sw} with SSS ($15.7 \pm 0.1\ \mu atm\,psu^{-1}$) by using the seven cruises presented here from 2006 to 2008 together with a zonal cruise performed in 2008 (2314 observations). The high agreement between both estimations suggests that the salinity dependence of fCO_{2sw} in the studied area remained very consistent from 2006 to 2013. Furthermore, these results point out that the Amazon River plume was the main driver of the observed fCO_{2sw} variability for the studied period.

Outside the direct influence of the Amazon River plume (hereby defined as SSS < 35 psu), the relationship between ln fCO_{2sw} and SST was calculated by linear regression and compared to the thermodynamic coefficient ($\frac{\partial fCO_2}{\partial SST} / fCO_2 = 0.0423°C^{-1}$, i.e., 4.23% $°C^{-1}$) [*Takahashi et al*., 1993; *Park and Wanninkhof* 2012]. Values of ln fCO_{2sw} versus SST close to the thermodynamic coefficient characterize areas where sea surface warming/cooling is

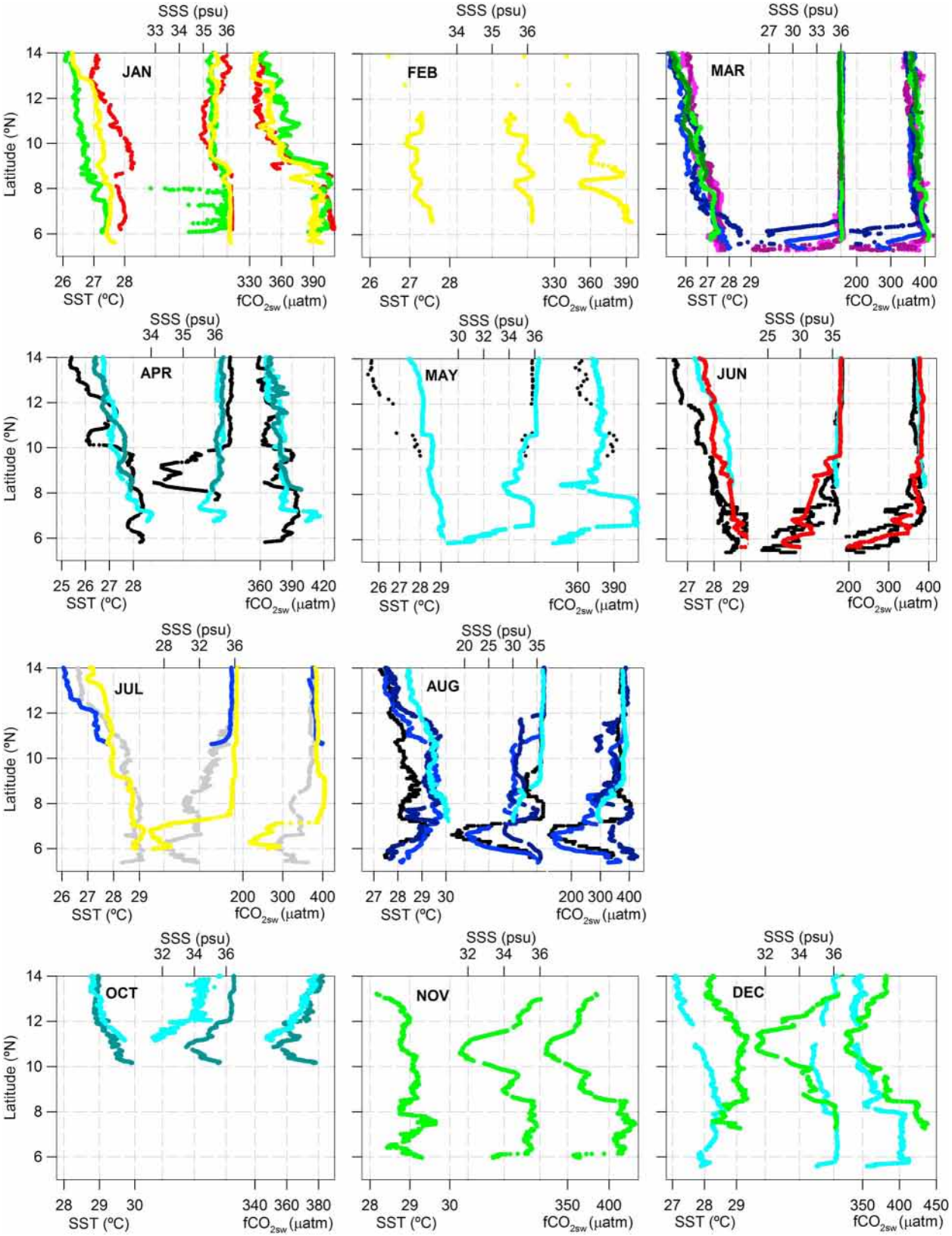

Figure 2. Latitudinal distribution of sea surface temperature (SST), sea surface salinity (SSS), and sea surface fCO_2 (fCO_{2sw}) for the 30 voyages of the *MN Colibri* used here. Each color represents a year: pink represents 2006, black 2007, grey 2008, blue 2009, cyan 2010, red 2011, green 2012, and yellow 2013. Light and dark colors were used when two voyages were performed during the same month of a year.

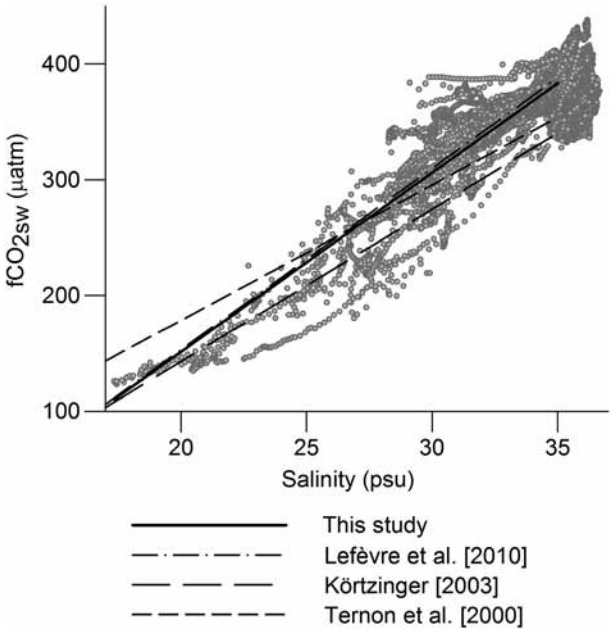

Figure 3. fCO_{2sw} as a function of SSS for the 30 voyages of the *MN Colibri*. Linear regression of fCO_{2sw} and SSS for salinities lower than 35 psu is shown (solid line) along with the relationships of *Ternon et al*. [2000], *Körtzinger* [2003], and *Lefèvre et al*. [2010] for the Amazon plume.

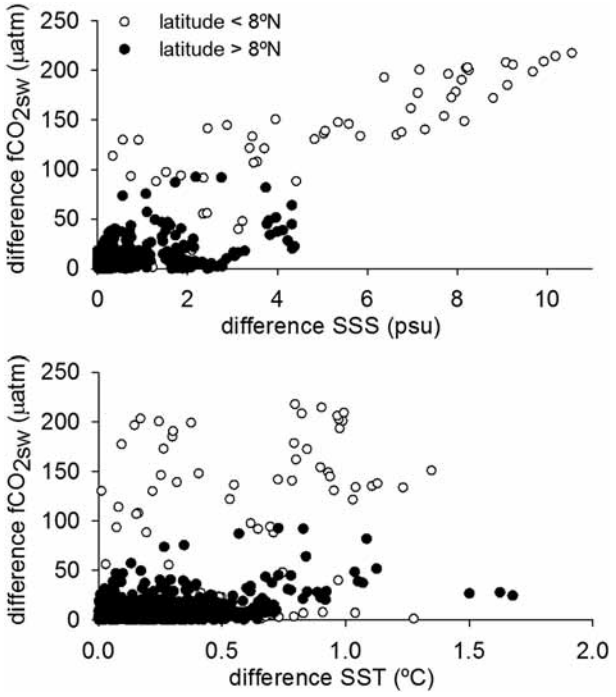

Figure 4. Comparison of the difference in fCO_{2sw}, salinity (SSS), and temperature (SST) among consecutive voyages of the *MN Colibri* with a time lag lower than a week between cruises. Values were averaged every 1/20 latitudinal degrees prior comparison. Data at latitudes lower than 8°N are represented with white dots, and black dots represent data at latitudes higher than 8°N.

the main factor explaining the observed fCO_{2sw} variability. In oceanic waters (SSS $>$ 35 psu), the coefficient of the fCO_{2sw}-SST relationship was lower than the thermodynamic coefficient (2.42 $\pm$ 0.03% $°C^{-1}$). Thus, both physical and biological processes seemed to act in shaping the fCO_{2sw} in the area outside the direct influence of the Amazon River plume. The net CO_2 outgassing at high SST would also be a factor contributing to the value of ln fCO_{2sw} versus SST lower than the thermodynamic coefficient.

3.2. Spatial Variability of SST, SSS, and fCO_{2sw}

The route of the *MN Colibri* was not consistent throughout the studied period (Figure 1). The paired cruises 1–2, 3–4, 8–9, 11–12, 13–14, 18–19, 20–21, 24–25, 26–27, and 28–29 were performed to and from Kourou at a time lag of less than 8 days (Table 1). Only paired cruises 3–4 and 28–29 used the same route, while the *MN Colibri* followed routes with up to 4° longitudinal distance at the northernmost limit of the studied area (14°N) in the remaining paired voyages. Thus, these paired cruises were used to evaluate the influence of the spatial variability between the tracks. The data measured on each cruise was first averaged into 1/20° latitudinal bins, and the absolute difference of SST, SSS, and fCO_{2sw} was calculated for each set of paired cruises (Figure 4). Significant differences were obtained for each set of paired cruises. SSS showed higher dispersion of the data when compared with SST, with maximum salinity discrepancies higher than 10 psu (lower than 2°C for SST). The northernmost limit observed in the brackish water (SSS $<$ 35 psu) transport along the coast (i.e., transported by the NBC, 8°N) was used to split the calculated differences (Figure 4). Despite the lower spatial distance among consecutive cruises when closer to Kourou (Figure 1), data collected south to 8°N showed the highest SSS and fCO_{2sw} discrepancy among consecutive tracks. The high number of surface eddies present in the region of the NBC retroflection, which is a significant path of

water transport in the area [*Ffield*, 2005], may be responsible for the high spatial variability found near the coast. On the other hand, north to 8°N, the range of variability of SSS, SST, and fCO_{2sw} during consecutive voyages was lower than that observed near the coast despite the higher zonal discrepancy among paired cruises.

The two cruises performed during October 2010 (cruises 18 and 19, Table 1) showed latitudinal SSS values in the study area consistently different. SSS from cruise 18 was lower and highly variable when compared to cruise 19 (Figure 2, October). Despite the robust correlation between SSS and fCO_{2sw} found at SSS < 35 psu in this study, fCO_{2sw} showed no significant differences among both cruises ($p < 0.001$). Water samples along the *MN Colibri* tracks were collected by the French Sea Surface Salinity Observation Service for salinity validation. During cruise 18, a blockage of the thermosalinograph installed on board the *MN Colibri*, which was solved before cruise 19, was identified as responsible for the deviation between the salinity measured on the collected samples and that measured on board. For the subsequent calculations, SSS from cruise 19 was interpolated at the latitudes where data were collected during cruise 18 and assigned to it.

3.3. Latitudinal Distribution of ΔfCO_2 Along the *MN Colibri* Tracks and Influence of the TNA Surface Water Circulation

As expected from the latitudinal distribution of fCO_{2sw}, ΔfCO_2 (the difference between fCO_{2sw} and fCO_{2atm}) showed high latitudinal variability (Figure 5). Stronger CO_2 undersaturation in surface waters was found during March, June, July, and August (lower than -200 µatm recorded during August) concomitant with the lowest SSS recorded. Outside the direct influence of the Amazon River plume, surface waters could be divided into two distinctive latitudinal zones corresponding to the ΔfCO_2 distribution: south of approximately 10°N, surface waters were characterized by the highest CO_2 oversaturation systematically recorded in all the voyages when brackish waters were not present (Figure 5). North of 10°N, a seasonal pattern was observed, with CO_2 undersaturation generally observed from January to April, although CO_2 oversaturation was also observed in some cruises (e.g., Figure 5). For the remaining period of the year, sea-air CO_2 exchange showed higher variability, with fCO_{2sw} close to fCO_{2atm}, which determined a highly variable latitudinal distribution of ΔfCO_2 (from August to December, a frontal zone was also observed close to 12°N probably associated to the northern limit of the Intertropical Convergence Zone, ITCZ, as it appears on SSS as well; Figure 2). Therefore, the ΔfCO_2 distribution suggests that these two regions corresponded to surface water masses with different origin.

Monthly mean zonal surface water velocities obtained from the Mercator Ocean GLORYS2V3 global ocean reanalysis are shown in Figure 5 for comparison with the latitudinal distribution of ΔfCO_2 (positive zonal velocities denote eastward propagation). The system of surface currents in the area is dominated by the NBC, the NECC, and the North Equatorial Current (NEC, Figure 1). From February to May/June, the NBC is transported northwestward feeding the Guyana Current, concomitant with a weakened NECC [*Johns et al*., 1998]. The interpolated zonal velocities for each of the *MN Colibri* tracks clearly show the weakness of the NECC from March until June (Figure 5). From approximately June to January, the NBC retroflection driven by the northward shift of the trade winds feeds the NECC with NBC waters, starting at between 5° and 8°N [*Fonseca et al*., 2004; *Garzoli et al*., 2004]. Additionally, the NEC retroflection can also contribute to the water transported eastward by the NECC [*Zhang et al*., 2003].

The interpolated latitudinal distribution of zonal surface water velocities along the *MN Colibri* tracks was used to explore the significance of the differences observed in the measured parameters in relation to the main sea surface current system. Thus, recorded values along the tracks with positive zonal velocities (eastward propagation) at latitudes higher than 8°N were associated to the NECC, and negative zonal velocities were associated to the NEC. Negative zonal velocities at latitudes lower than 8°N were associated to the NBC. Recorded data with SSS lower than 35 psu were excluded from this analysis to minimize the interference of the Amazon River plume in the characterization of the oceanic waters present in the studied area. Furthermore, the three cruises performed during 2013 were excluded from this analysis due to the lack of surface velocity data.

Under the imposed constraints, averaged SSS associated to the NECC at each cruise of the *MN Colibri* was significantly lower than that associated to the NEC (paired *t* test $p < 0.01$, $n = 23$). No other significant differences regarding SSS were found among the three main currents present in the area ($p > 0.4$). Averaged SST and fCO_{2sw} associated to the NECC were significantly higher than those found for the NEC ($p < 0.0001$; $n = 23$; Figure 6a,

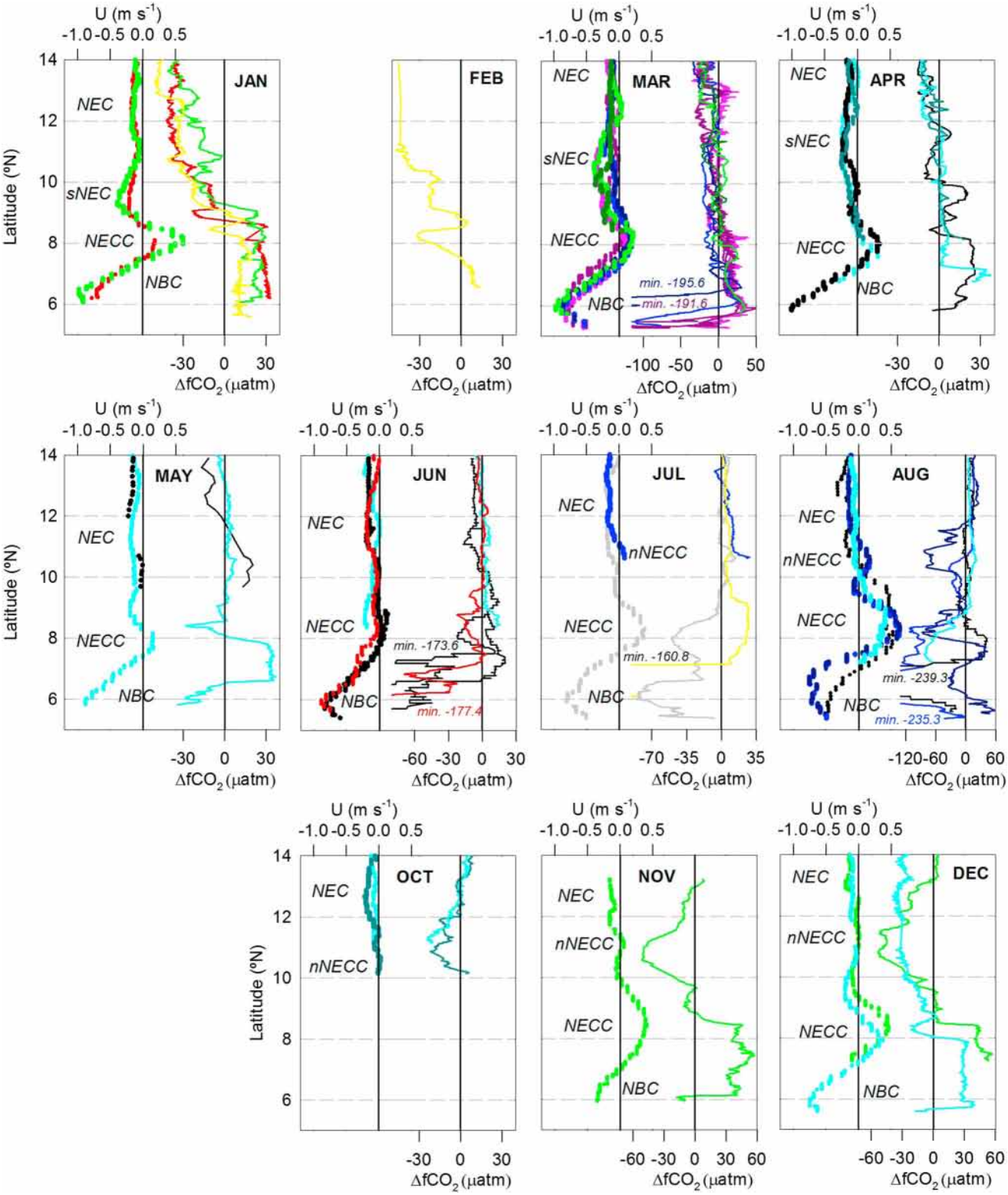

Figure 5. Distribution of the calculated ΔfCO_2 between 14 and 5°N along the tracks of the *MN Colibri*. Monthly-averaged surface zonal velocity (*U*) interpolated at each point where measurements were taken along the *MN Colibri* tracks is also shown for comparison. Positive zonal velocities denote eastward propagation. Each color represents a year: pink represents 2006, black 2007, grey 2008, blue 2009, cyan 2010, red 2011, green 2012, and yellow 2013. Dark and light colors were used when two voyages were performed during the same month of a year.

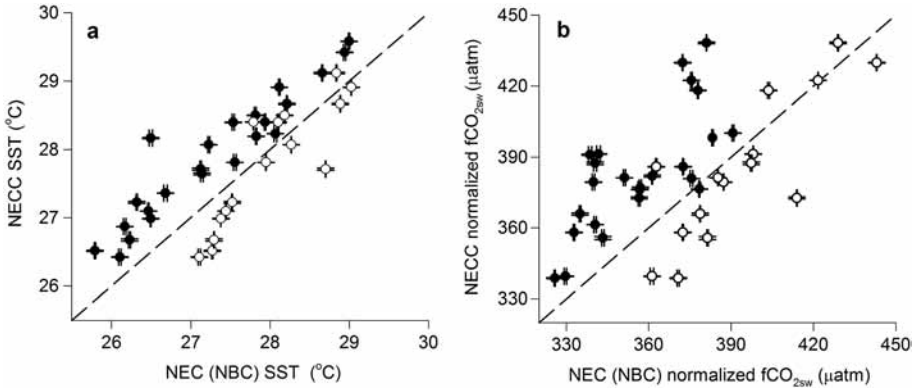

Figure 6. Comparison of cruise-averaged (a) SST and (b) temperature and salinity-normalized fCO_{2sw} associated to the main surface currents present in the studied area: NBC, NECC, and NEC. Black dots represent the comparison between the NEC and the NECC, while white dots represent the comparison between the NBC and the NECC. Dashed lines represent the 1:1 relationship. Error bars represent the standard error of the estimate.

black dots). Cruise-averaged SST associated to the NEC ranged from 25.8 to 29.0°C (average 27.4 ± 0.2°C), while mean SST ranged from 26.4 to 29.6°C in the NECC (average 28.0 ± 0.2°C). Furthermore, averaged SST was not significantly different between the NECC and the NBC ($p > 0.08$; $n = 15$; Figure 6a, white dots). Due to the important SST and SSS differences found between the NECC (NBC) and the NEC, the thermodynamic dependence of fCO_{2sw} with SSS and SST was used to remove the temperature and salinity effects over the observed fCO_{2sw} [*Takahashi et al.*, 1993]. The mean SST from all the data presented here was used as reference value (27.7°C; $n = 27975$) for SST normalization of the fCO_{2sw}. The thermodynamic effect of SSS over the observed fCO_{2sw} was used to normalize the data to a SSS of 35 psu by using $(\partial fCO_2/\partial SSS)/(SSS/fCO_2) = \gamma_s$, where γ_s is the thermodynamic factor. The thermodynamic effect of SSS over fCO_{2sw} reflects the changes in the solubility of CO_2 and in the dissociation constants of carbonic acid. This effect is not well constrained as it depends on several factors, resulting in reported γ_s values ranging from 0.93 to 1.7. Higher γ_s values reflect the thermodynamic effect of SSS over fCO_{2sw} when resulting from the admixture of waters with significantly different TCO_2 content, such as the influence of rainfall on seawater [*Sarmiento and Gruber*, 2006]. Here the influence of the Amazon River plume is assumed negligible since fCO_{2sw} values associated to SSS < 35 psu were removed from this analysis. Thus, the γ_s value reported by *Takahashi et al.* [1993] for warm waters and for a SSS range of 33.5 to 37 psu was used ($\gamma_s = 0.93$). SSS and SST differences could not explain the different fCO_{2sw} (and consequently ΔfCO_2) associated to the NECC (NBC) compared to the NEC (Figure 6b). SSS and SST-normalized fCO_{2sw} associated to the NECC (and NBC) were significantly different to those associated to the NEC ($p < 0.0001$), whereas no significant differences were found in the normalized fCO_{2sw} associated to the NBC and the NECC ($p > 0.5$). Thus, these results indicate that the NBC is the main contributor to the NECC in the studied area throughout the year.

In a series of transects performed farther east in the tropical Atlantic, *Lefèvre et al.* [2014] observed that the warm waters associated to the SEC presented permanent strong CO_2 oversaturation despite the seasonal influence of the Intertropical Convergence Zone (ITCZ). These waters are associated to the equatorial upwelling system and are transported westward by the SEC toward the Brazilian coast, feeding the NBC [*Stramma and Schott*, 1999]. Thus, the spread of Southern Hemisphere waters in the TNA that transports CO_2-rich waters originated from the equatorial upwelling system is the most probable explanation for the permanent CO_2 oversaturation associated to the NBC and the NECC. Despite the CO_2 outgassing and the cooling effect as these waters were transported from the southeast tropical Atlantic into the studied area, permanent seawater CO_2 oversaturation remained effective throughout the year, only dramatically changed by the influence of the Amazon River plume.

3.4. Seasonal Variability of ΔfCO_2 and Resulting Sea-Air CO_2 Fluxes in the TNA

The main driver of spatial variability along the tracks of the *MN Colibri* was related to the location of the Amazon River plume affected by mesoscale circulation rather than the meridional discrepancy of the tracks. Thus, for the evaluation of the seasonal changes, the influence of the meridional discrepancy among tracks

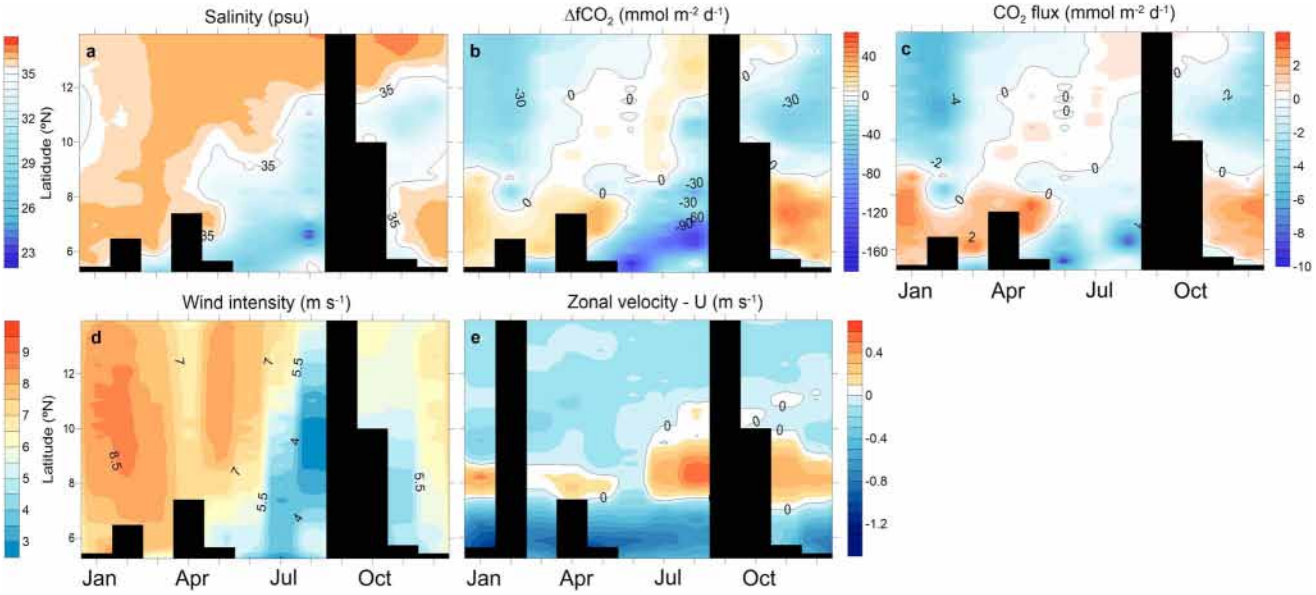

Figure 7. Monthly-averaged latitudinal distribution of (a) sea surface salinity, (b) ΔfCO_2, (c) resulting sea-air CO_2 fluxes, (d) interpolated wind intensity, and (e) the zonal component of the surface water velocity. Positive zonal velocities denote eastward propagation and are associated to the NECC in the studied area. Data were averaged every 0.1° of latitude. Black areas represent zones with no data.

was assumed negligible. Monthly means of SSS, ΔfCO_2, sea-air CO_2 fluxes, wind intensity, and the zonal component of the surface water velocity were computed by averaging the data at every 0.1° of latitude for each month (Figure 7).

Monthly-averaged SSS and ΔfCO_2 reflected the latitudinal distribution of the main surface water currents and the seasonal change in the transport of the Amazon River plume (Figure 7). The NBC retroflection transported brackish waters and the associated CO_2 undersaturation to the north during the second half of the year (Figures 7a and 7b). On the other hand, the maximum CO_2 oversaturation in surface waters was permanently located south to 10°N throughout the year, in the area influenced by the NBC and the NECC (Figure 7e). In the area where NEC dominated the surface water transport (12–14°N; Figure 7e), surface waters acted on average as a source of CO_2 to the atmosphere from May to October/November and a sink the rest of the year. The thermodynamic effect of SST variations largely explained the seasonal pattern in the sea-air CO_2 exchange in the NEC. The cooling of surface waters during boreal winter led to the reversing of the direction of the CO_2 fluxes at the sea-air interface.

Calculated, monthly mean sea-air CO_2 fluxes ranged from 3.7 to -11.0 mmol m^{-2} d^{-1} (Figure 7c). The seasonal northward shift of the trade winds, which is responsible for the start of the NBC retroflection, promoted a wind intensity relaxation in the second half of the year (Figure 7d). As a consequence, the seasonal wind intensity change had an important impact on the sea-air CO_2 fluxes. The monthly mean CO_2 oversaturation observed in the NBC and the NECC from January to May was less pronounced than that observed during November and December. Nevertheless, the higher wind intensity during the first half of the year drove higher CO_2 outgassing during this period when compared to November and December. A similar influence of the seasonality in the wind field was observed in the NEC: equivalent CO_2 undersaturation found during January–February and November–December in the NEC (Figure 7b) resulted in higher atmospheric CO_2 absorption during January–February due to the increase in wind intensity.

The studied area acted as a net sink of atmospheric CO_2 (Table 2), mainly driven by the CO_2 undersaturation promoted by the Amazon River plume and also due to the seasonal pattern identified in the NEC. Monthly-averaged sea-air CO_2 fluxes ranged from -72.2 ± 10.2 mmol m^{-2} $month^{-1}$ in February to 14.3 ± 4.5 mmol m^{-2} $month^{-1}$ in May. Although the higher latitudinal distribution of the Amazon River plume occurred during the second half of the year, when the NBC retroflection took place, maximum atmospheric CO_2 absorption occurred during boreal winter (January–February). During these months, the NEC acted as a sink of atmospheric CO_2,

Table 2. Estimated Monthly Sea-Air CO_2 Flux Derived From the Monthly Means Calculated for the Study Area[a]

	This Study	*Takahashi et al.* [2009]	*Landschützer et al.* [2014]
	($mmol\ m^{-2}\ month^{-1}$)		
January	−42.7 ± 10.9	46.4 ± 38.4	−3.8 ± 10.1
February	−72.2 ± 10.2	−2.0 ± 50.6	−10.6 ± 10.3
March	−8.1 ± 5.7	28.2 ± 24.2	−12.7 ± 7.5
April	−1.1 ± 2.8	11.6 ± 14.9	0.6 ± 6.7
May	14.3 ± 4.5	20.9 ± 14.4	16.0 ± 5.8
June	−31.5 ± 7.1	54.4 ± 15.9	24.8 ± 4.2
July	−3.6 ± 2.3	42.4 ± 3.1	15.3 ± 0.9
August	−29.8 ± 7.7	35.0 ± 3.4	9.2 ± 1.6
October	−10.9 ± 2.7	30.4 ± 7.4	3.6 ± 1.4
November	−4.4 ± 5.6	16.5 ± 17.6	1.4 ± 1.9
December	−23.7 ± 7.3	41.9 ± 19.0	1.7 ± 5.9

[a]Monthly sea-air CO_2 flux for the study area computed from the climatology of *Takahashi et al.* [2009] (reference year 2000) and that presented by *Landschützer et al.* [2014] (reference year 2010) are also shown. September is absent due to the lack of cruises of the *MN Colibri* during this month.

which together with the CO_2 undersaturation caused by the Amazon River plume and the increase in the wind velocity during the first half of the year, caused the strong atmospheric CO_2 absorption.

Seasonal sea-air CO_2 fluxes calculated here were compared with the sea-air CO_2 flux climatologies of *Takahashi et al.* [2009] and *Landschützer et al.* [2014] made for the reference year 2000 and 2010, respectively (Table 2). Comparison of the results presented here with the climatology of *Takahashi et al.* [2009] (4° × 5° resolution) was made by integrating the pixels contained within the area covered by the different tracks of the *MN Colibri* (i.e., 5 pixels). As the climatology of *Landschützer et al.* [2014] presents a much finer spatial resolution (1° × 1° resolution), the integration of the pixels contained within the averaged track of the *MN Colibri* was used for comparison (16 pixels). With the only exception of February, the climatology of *Takahashi et al.* [2009] estimated a net CO_2 efflux from surface waters in the studied area throughout the year (Table 2). The climatology of *Landschützer et al.* [2014], based on the Surface Ocean CO_2 Atlas (SOCAT) database [*Bakker et al.*, 2014], also characterized the area as a net source of CO_2 to the atmosphere (Table 2). Both climatologies reproduced the seasonal pattern identified in the NEC (data not shown) but were not able to reproduce the magnitude and extent of the CO_2 undersaturation caused by the Amazon River plume. The high spatial extent of the CO_2 undersaturation associated to the Amazon River plume, the coarser spatial resolution of the climatology of *Takahashi et al.* [2009], and the scarce fCO_{2sw} data in the area might be responsible for the strong disagreement between both sea-air CO_2 flux climatologies and our results. The significance of the Amazon River plume in terms of atmospheric CO_2 uptake has been highlighted in previous studies [*Körtzinger*, 2003; *Cooley et al.*, 2007; *Lefèvre et al.*, 2010] and roughly represents 10% of the total CO_2 outgassing estimated for the tropical Atlantic. Results suggest that the Amazon River plume should be taken into account to better constraint the role of the tropical Atlantic in the global sea-air CO_2 exchange.

3.5. Origin of the CO_2 Undersaturation in the Amazon River Plume

The upper Amazon River acts as a source of CO_2 to the atmosphere largely supported by the export of both inorganic and organic carbon from flooded wetlands and organic matter mineralization along the river path [e.g., *Abril et al.*, 2014]. As in other major river systems, the Amazon River progressively changes its role downstream and becomes a net sink of atmospheric CO_2 in the coastal ocean [*Chen et al.*, 2012]. The linear relationship between fCO_{2sw} and SSS within the plume determined here (Figure 3) presented a negative intercept at zero salinity, which suggests that the CO_2 undersaturation originated from the midsalinity range. Primary production at this mixing zone could contribute to the observed CO_2 undersaturation but, as shown by *Körtzinger* [2010], the nonlinearity of the thermodynamics of the CO_2 system alone permits a CO_2 undersaturation zone to develop in the mixing zone of CO_2 saturated seawater and CO_2 supersaturated river waters. To evaluate the role of physical versus biological processes in explaining the permanent CO_2 undersaturation of the Amazon River plume, *Ternon et al.* [2000] and *Körtzinger* [2003] compared their TA, TCO_2, and fCO_{2sw} data with curves resulting from the conservative mixing of Amazon River waters and the surrounding oceanic waters using the composition of the end-members given in Table 3. As the observed fCO_{2sw} values

Table 3. Main Characteristics of the Freshwater and Seawater End-Members Used by *Ternon et al.* [2000], *Körtzinger* [2003], and This Study for the Calculation of the Mixing Effect Between the Amazon River and the Tropical Atlantic Over the Observed fCO_{2sw}[a]

Reference	Silicates (μmol/kg)	Phosphates (μmol/kg)	Temperature (°C)	Salinity (psu)	TCO_2 (μmol/kg)	TA (μmol/kg)
Ternon et al. [2000]	142		28	0	600	600
Körtzinger [2003]	150	0.8	29	0	744	600
April 2013	n.m.	n.m.	29	1.08	397.7	322.3
Ternon et al. [2000]	2	0	28	36.2	2018	2403
Körtzinger [2003]	1.5	0	29	34.9	1948	2306
October 2012	n.m.	n.m.	29	36	2020	2360

[a]n.m. denotes not measured properties.

were lower than those expected from conservative mixing, they concluded that biological processes were responsible for the CO_2 undersaturation found in the Amazon River plume.

Due to the difficulty in defining the characteristics of the Amazon River end-member, uncertainty remains about the relative contribution of mixing versus biological activity in explaining the permanent CO_2 undersaturation associated to the Amazon River plume. In April 2013, TA and TCO_2 were measured at a salinity of 1.08 psu in the transect performed perpendicular to the Amazon River mouth (Figures 8a and 8b; Table 3). These values were compared with the linear relationships of TA and TCO_2 with SSS found by *Lefèvre et al.* [2010] who included the data used by *Ternon et al.* [2000] (Figures 8a and 8b). TA measured during the transect performed in 2013 at $S = 1.08$ psu was in good agreement with the value given by the TA-SSS correlation found by *Lefèvre et al.* [2010] (Figure 8a):

$$TA = 58.1 * SSS + 265 \quad (5)$$

This suggests that TA acted conservatively during the mixing between the Amazon River and the oceanic waters.

On a similar fashion, TCO_2 measured in April 2013 was compared with the linear relationship of TCO_2 and SSS found by *Lefèvre et al.* [2010]. The linear relationship of TCO_2 and SSS found by *Lefèvre et al.* [2010] gave a TCO_2 of 244 μmol kg^{-1} at 1.08 psu, contrasting with the much higher value measured (398 μmol kg^{-1}; Table 3). This suggests a biological CO_2 uptake of 154 μmol kg^{-1} within the early Amazon River plume.

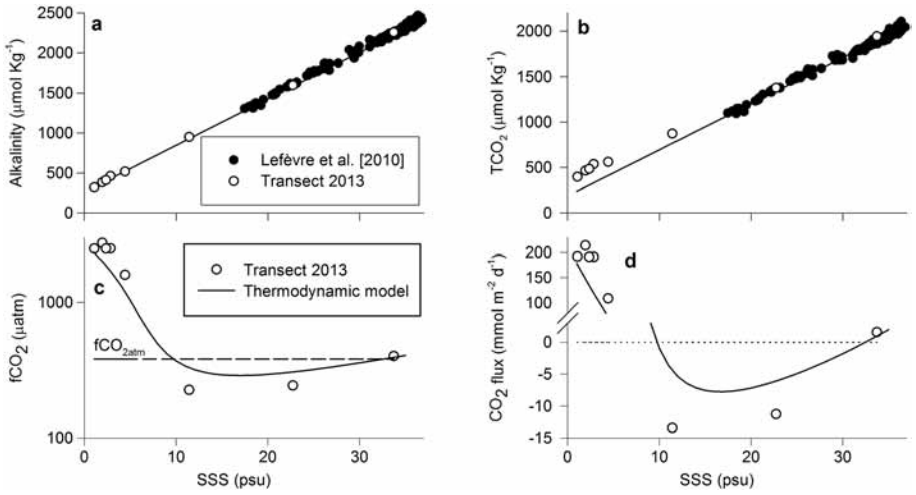

Figure 8. (a) TA and (b) TCO_2 as a function of SSS in the transect performed near the river mouth during April 2013 (white dots). The measurements made within the Amazon plume and presented in *Lefèvre et al.* [2010] are also represented (black dots). (c) Distribution of calculated fCO_{2sw} as a function of SSS for the water samples collected in the transect performed during April 2013 together with that predicted by the mixing-only thermodynamic model. The calculated fCO_{2atm} for the period when the samples were taken is also shown (dashed line). (d) Resulting sea-air CO_2 fluxes calculated from the samples collected in April 2013 and those resulting from the thermodynamic model.

fCO_{2atm} in the Amazon River plume can be roughly estimated to ~390 μatm during the period the *MN Colibri* cruises were performed. During the cruise Camadas Finas 2, performed in October 2012, fCO_{2sw} close to atmospheric values was observed at SSS ~36 psu. This corresponded to $TCO_2 \sim 2020\ \mu mol\ kg^{-1}$ and TA ~2360 $\mu mol\ kg^{-1}$, hereby defined as the seawater end-member. Using the seawater end-member and the TCO_2 value measured during the transect performed during 2013 at the lowest SSS (1.8 psu), the mixing equation for TCO_2 becomes

$$TCO_2 = 46.46 * SSS + 347.5 \quad (6)$$

This characterizes the freshwater end-member with $TCO_2 = 347.5\ \mu mol\ kg^{-1}$ at 0 psu.

The discrepancy between our mixing equations and those presented in *Ternon et al*. [2000] was mainly due to the TA and TCO_2 values assigned to the freshwater end-member. The TA value reported here as Amazon River end-member was within the range of TA values given by *Gibbs* [1972] (247–551 $\mu mol\ kg^{-1}$). Furthermore, the TA and TCO_2 measurements performed in April 2013 gave a calculated fCO_{2sw} over 2500 μatm at the lowest salinity measured (Figure 8c), which is consistent with the strong CO_2 outgassing observed within the Amazon River in previous studies [*Richey et al*., 2002; *Abril et al*., 2014].

The theoretical fCO_{2sw} resulting from the mixing equations of TA and TCO_2 presented here was calculated for the conditions found in the Amazon River plume (SSS, SST, and atmospheric pressure). For this, we used the thermodynamic relationships of the CO_2 system in aquatic environments [*Mojica Prieto and Millero*, 2002] and assumed no CO_2 exchange with the atmosphere [*Körtzinger*, 2010]. As shown by *Körtzinger* [2010], mixing alone could lead to CO_2 undersaturation due to the nonlinear thermodynamics of the CO_2 system (Figure 8c). Nevertheless, the calculated fCO_{2sw} from our measurements made in April 2013 significantly deviated from the thermodynamic model (Figure 8c). In the midsalinity range, the observed CO_2 undersaturation was stronger than that predicted by mixing alone. As a consequence, at a SSS of 11.4 psu, biological CO_2 drawdown was responsible for a CO_2 flux of $-8.6\ mmol\ m^{-2}\ d^{-1}$ (i.e., 64% of the total $-13.4\ mmol\ m^{-2}\ d^{-1}$ observed).

Although the assumption of no CO_2 exchange with the atmosphere in the thermodynamic model presented could lead to deviations in the contribution of abiotic factors to the CO_2 undersaturation in the Amazon plume, the time scale of CO_2 equilibration is much larger than the propagation of the plume at the spatial scale of the transect of April 2013 [*Körtzinger*, 2010]. Furthermore, at salinities lower than 10 psu, the fCO_{2sw} observed during April 2013 was higher than that calculated by the mixing model, which could be attributed to the dominance of organic matter mineralization near the River mouth. Thus, the calculated contribution of primary production to the observed CO_2 undersaturation at the midsalinity range is a conservative estimation.

Despite the high spatial variability of the Amazon River plume as shown in the analysis of the data from consecutive cruises presented here, interpolated, monthly-averaged chlorophyll *a* derived from the MODIS/aqua satellite showed high significant correlation with measured SSS in 22 of the 30 voyages of the *MN Colibri* (Figure 9). In these cruises, apparent chlorophyll *a* concentration within the Amazon River plume could be up to 2 orders of magnitude higher than in the surrounding oceanic waters. The oceanic waters of the tropical Atlantic present permanent oligotrophic conditions which explain the presence of low-chlorophyll *a* concentration [*Subramaniam et al*., 2008]. The spread of Amazon waters in the area dramatically changes this content, providing the conditions to sustain important N_2 fixation and primary production [*Subramaniam et al*., 2008], thus explaining the resilience of the permanent atmospheric CO_2 sink associated to the Amazon River plume.

3.6. Interannual Variability of Sea-Air CO_2 Fluxes in the TNA

The spatial extent of the Amazon River plume and the associated CO_2 undersaturation depend on factors like river discharge, wind intensity, and the magnitude of the local system of surface currents [*Molleri et al*., 2010]. Large-scale, climatic events exert an important control over precipitation and wind intensity (and therefore the system of surface currents) in the western tropical Atlantic and the Amazon River basin. Precipitation anomalies in the Amazon basin have been related to the El Niño–Southern Oscillation (ENSO), resulting in increased (reduced) river discharge during La Niña (El Niño) events (Figure 10) [*Sombroek*, 2001]. The ENSO variability is also known to have a remote influence on the tropical Atlantic climate variability [e.g., *Alexander and Scott*, 2002; *Rodrigues and McPhaden*, 2014]. Warming of the tropical Pacific during El Niño events produces a warming in the troposphere which then propagates eastward, generally promoting positive SST anomalies in the tropical Atlantic with a time lag of a few months [*Alexander and Scott*, 2002; *Chiang and Sobel*, 2002].

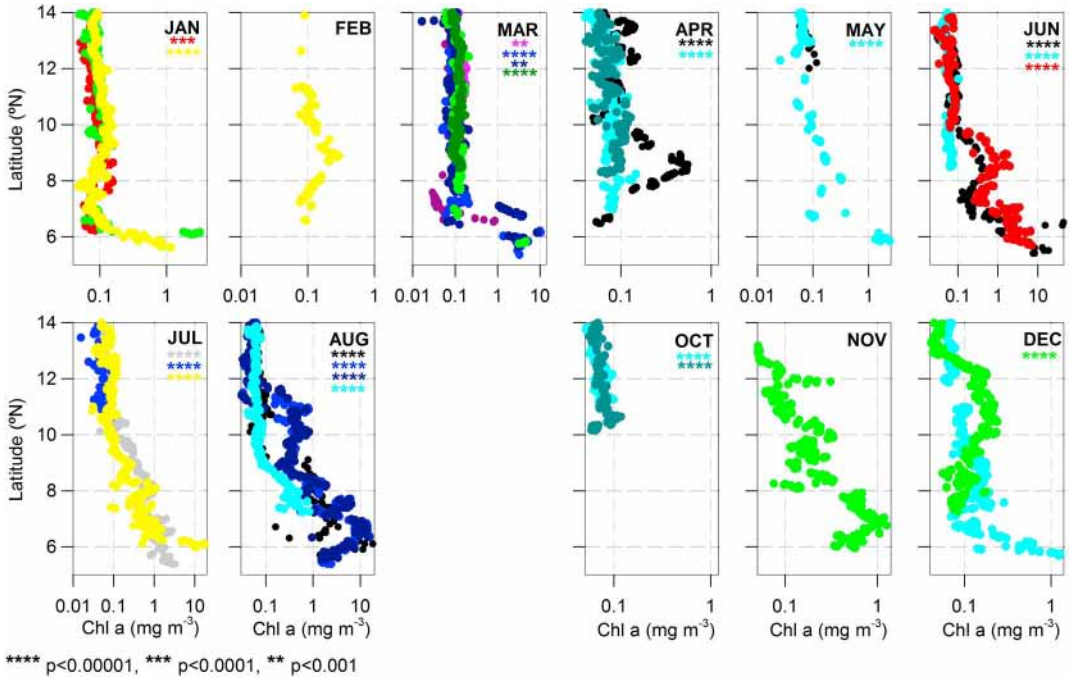

Figure 9. Monthly-averaged chlorophyll *a* concentration in surface waters obtained from the MODIS/Aqua satellite and interpolated at each point where measurements were taken along the *MN Colibri* tracks. The significance of the Spearman correlation between the SSS measured along the *MN Colibri* tracks and the interpolated monthly-averaged chlorophyll *a* concentration is also shown. Note the logarithmic scale in the chlorophyll *a* concentration.

The zonal component of the surface water circulation used here (Figure 5) was used to obtain the averaged SST anomalies associated to each sea surface current (after excluding salinities lower than 35 psu). SST anomalies showed significant lagged correlation with the NINO3.4 index. Maximum positive correlation between SST anomalies associated to the three main currents in the area and the NINO3.4 index was obtained with a time lag of 6 months (Spearman's $\rho = 0.53$, $n = 65$, and $p < 0.00001$). Furthermore, SST anomalies associated to each individual sea surface current were also significantly correlated with the NINO3.4 index. Maximum correlation of SST anomalies associated to each sea surface current with the NINO3.4 index was also found with a time lag of 6 months (NEC: $\rho = 0.44$, $n = 27$, and $p < 0.05$; NECC: $\rho = 0.61$, $n = 23$, and $p < 0.005$; NBC: $\rho = 0.61$, $n = 15$, and $p < 0.05$).

The year 2010 was of significant changes in the tropical Atlantic and the Amazon River basin: a severe drought in the Amazon River basin led to the lowest River discharge rates of the studied period, concomitant

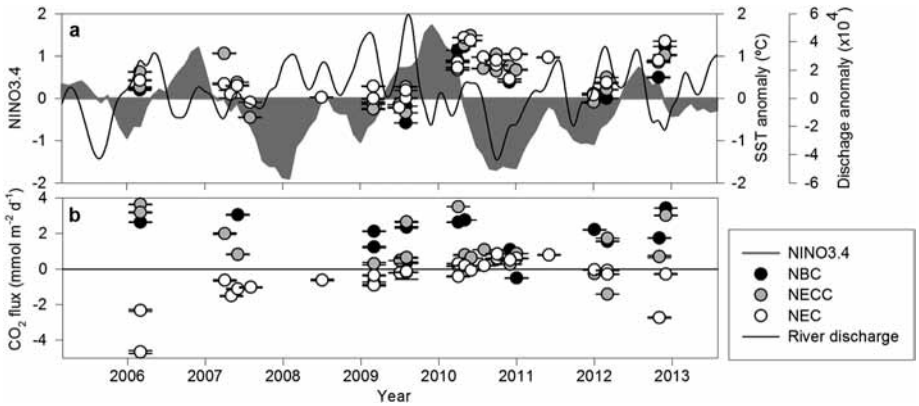

Figure 10. (a) Computed SST anomalies for the three main surface currents present in the studied area. Amazon River discharge anomalies and the NINO3.4 index are also shown for comparison. (b) Temporal evolution of calculated CO_2 fluxes for each of the three main surface currents present in the studied area. Error bars represent the standard error of the estimate.

with positive SST anomalies in the three sea surface currents present in the studied area (Figure 10). SST changes can induce rapid changes in the sea-air CO_2 fluxes. Whereas the NBC and the NECC acted as almost permanent sources of CO_2 to the atmosphere throughout the studied period, the NEC showed to be more sensitive to SST changes (Figure 10). SST has an important effect over the CO_2 fluxes in the NEC, driving the seasonal change in the direction of the CO_2 fluxes as discussed before. Nevertheless, the temporal evolution of the sea-air CO_2 fluxes in the NEC reveals that it acted as a net source of CO_2 to the atmosphere during 2010 and early 2011. This contrasts with the other years explored here where the NEC acted as a net sink of atmospheric CO_2 or it was in near equilibrium with the atmospheric CO_2 (Figure 10).

By analyzing underway fCO_2 data measured on board a merchant ship performing the route France-Brazil farther east in the tropical Atlantic, *Lefèvre et al.* [2013] identified an increased CO_2 outgassing in the boreal spring of 2010 compared to 2009 and 2011 in the 8°S to 8°N latitudinal band. Positive SST anomalies concomitant with positive SSS anomalies caused by the northward shift of the ITCZ were identified as responsible for this increased CO_2 outgassing. As the NEC extends farther north of the studied area until approximately 20–25°N, the results presented here suggest that the CO_2 outgassing caused by the anomalous climatic conditions of 2010 may have a much larger impact on the sea-air CO_2 exchange in the tropical Atlantic.

4. Conclusions

Global sea-air CO_2 flux climatologies identify the studied area (5–14°N, 41–52°W) as a net source of CO_2 to the atmosphere. The results presented here showed that the spatial extent of the Amazon River plume together with the seasonality in the sea-air CO_2 exchange in the NEC characterized the studied area as a net sink of atmospheric CO_2. In the case of the Amazon River plume, its spread in the western TNA changed the permanent CO_2 oversaturation of the oceanic waters transported by the NBC and the NECC and largely affected the sea-air CO_2 exchange in the western tropical Atlantic. Intense primary production promoted by the river discharge seemed to be the main driver of the observed CO_2 undersaturation within the Amazon River plume. Net primary production within the inner plume was shown to reverse the CO_2 oversaturated conditions of the Amazon waters and develop CO_2 undersaturated conditions near the River mouth. This CO_2 drawdown was associated to a significant increase in the satellite-derived chlorophyll *a* concentration.

The combination of measured fCO_2 data with interpolated surface water zonal velocities permitted to identify the influence of surface water circulation on the sea-air CO_2 fluxes in the area. Results demonstrated the presence of two distinctive surface water masses with different fCO_{2sw} characteristics. As a result, CO_2-rich waters probably originated from the equatorial upwelling system spread in the TNA carried by the NBC and the NECC. These waters were characterized as permanent sources of CO_2 to the atmosphere throughout the studied period. On the other hand, surface water transported by the NEC showed to be more sensitive to SST changes, determining not only the seasonality in the direction of the CO_2 fluxes at the sea-air interface but also the impact of large climatic events such as the ENSO on the sea-air CO_2 exchange in the region.

The data used in this study have proved that regular monitoring of CO_2 in the ocean permits to investigate the seasonal and interannual variability of the sea-air CO_2 exchange. This is particularly important regarding the current and projected environmental changes in the area such as increasing SST or changes in the equatorial upwelling that will alter the CO_2 exchange in the tropical Atlantic. Thus, CO_2 monitoring programs are crucial for better understanding the dynamics of CO_2 in the oceans and the impact of climate variability on the sea-air CO_2 exchange and carbon storage in the oceans.

Acknowledgments

We acknowledge the Compagnie Maritime Nantaise (MN) for allowing the installation of the CO_2 equipment on board their ship. Analysis of dissolved inorganic carbon and alkalinity in the water samples was performed by the SNAPO-CO_2 at LOCEAN. Chlorophyll *a* data were downloaded from the Giovanni online data system, developed and maintained by the NASA Goddard Earth Sciences (GES) Data and Information Services Center (DISC). Temperature and surface water zonal velocities were downloaded from the MyOcean system, maintained by the MyOcean 2 project and included in the integrated pan-European Marine Core Service for ocean monitoring and forecasting. Data derived from the NCEP reanalysis project was provided by the NOAA/OAR/ESRL PSD, Boulder, Colorado, USA (http://www.esrl.noaa.gov/psd/). Sea surface salinity data derived from thermosalinograph instruments installed on board voluntary observing ships were collected, validated, archived, and made freely available by the French Sea Surface Salinity Observation Service (http://www.legos.obs-mip.fr/observations/sss/). We thank the support from the European Integrated Projects CARBOOCEAN (contract 511176–2) and CARBOCHANGE (FP7 264879), the Brazilian National Institute of Science and Technology in Tropical Marine Environments, INCT-AmbTropic (CNPq/FAPESB grants: 565054/2010-4 and 8936/2011), the BIOAMAZON project, and the Institut de Recherche pour le Developpement (IRD). J.S.P.I. was supported by a postdoctoral fellowship from the CARBOCHANGE project. The fCO_2 data presented here are partially available in the SOCAT v2 database. The remaining data will be available in the upcoming SOCAT v3. We thank the anonymous reviewer who helped in improving the original version of the manuscript.

References

Abril, G., et al. (2014), Amazon River carbon dioxide outgassing fuelled by wetlands, *Nature*, *505*(7483), 395–398, doi:10.1038/nature12797.

Alexander, M., and J. Scott (2002), The influence of ENSO on air-sea interaction in the Atlantic, *Geophys. Res. Lett.*, *29*(14), 46–1, doi:10.1029/2001GL014347.

Andrié, C., C. Oudot, C. Genthon, and L. Merlivat (1986), CO_2 fluxes in the tropical Atlantic during FOCAL cruises, *J. Geophys. Res.*, *91*(C10), 11,741–11,755, doi:10.1029/JC091iC10p11741.

Bakker, D. C. E., et al. (2014), An update to the Surface Ocean CO_2 Atlas (SOCAT version 2), *Earth Syst. Sci. Data*, *6*(1), 69–90, doi:10.5194/essd-6-69-2014.

Chen, C.-T. A., T.-H. Huang, Y.-H. Fu, Y. Bai, and X. He (2012), Strong sources of CO_2 in upper estuaries become sinks of CO_2 in large river plumes, *Curr. Opin. Environ. Sustainability*, *4*(2), 179–185, doi:10.1016/j.cosust.2012.02.003.

Chiang, J. C. H., and A. H. Sobel (2002), Tropical tropospheric temperature variations caused by ENSO and their influence on the remote tropical climate, *J. Clim.*, *15*(18), 2616–2631, doi:10.1175/1520-0442(2002)015<2616:TTTVCB>2.0.CO;2.
Coles, V. J., M. T. Brooks, J. Hopkins, M. R. Stukel, P. L. Yager, and R. R. Hood (2013), The pathways and properties of the Amazon River plume in the tropical North Atlantic Ocean, *J. Geophys. Res. Oceans*, *118*, 6894–6913, doi:10.1002/2013JC008981.
Cooley, S. R., V. J. Coles, A. Subramaniam, and P. L. Yager (2007), Seasonal variations in the Amazon plume-related atmospheric carbon sink, *Global Biogeochem. Cycles*, *21*, GB3014, doi:10.1029/2006GB002831.
Department of Energy (1994), Handbook of methods for the analysis of the various parameters of the carbon dioxide system in sea water, ORNL/CDIAC-74.
Edmond, J. M. (1970), High precision determination of titration alkalinity and total carbon dioxide content of sea water by potentiometric titration, *Deep Sea Res. Oceanogr. Abstr.*, *17*(4), 737–750, doi:10.1016/0011-7471(70)90038-0.
Ffield, A. (2005), North Brazil current rings viewed by TRMM Microwave Imager SST and the influence of the Amazon Plume, *Deep Sea Res., Part I*, *52*(1), 137–160, doi:10.1016/j.dsr.2004.05.013.
Fonseca, C. A., G. J. Goni, W. E. Johns, and E. J. D. Campos (2004), Investigation of the North Brazil Current retroflection and North Equatorial Countercurrent variability, *Geophys. Res. Lett.*, *31*, L21304, doi:10.1029/2004GL020054.
Garzoli, S. L., A. Ffield, W. E. Johns, and Q. Yao (2004), North Brazil Current retroflection and transports, *J. Geophys. Res.*, *109*, C01013, doi:10.1029/2003JC001775.
Gibbs, R. J. (1972), Water chemistry of the Amazon River, *Geochim. Cosmochim. Acta*, *36*(9), 1061–1066, doi:10.1016/0016-7037(72)90021-X.
Johns, W. E., T. N. Lee, R. C. Beardsley, J. Candela, R. Limeburner, and B. Castro (1998), Annual cycle and variability of the North Brazil Current, *J. Phys. Oceanogr.*, *28*(1), 103–128, doi:10.1175/1520-0485(1998)028<0103:ACAVOT>2.0.CO;2.
Kirchner, K., M. Rhein, S. Hüttl-Kabus, and C. W. Böning (2009), On the spreading of south Atlantic water into the Northern Hemisphere, *J. Geophys. Res.*, *114*, C05019, doi:10.1029/2008JC005165.
Körtzinger, A. (2003), A significant CO_2 sink in the tropical Atlantic Ocean associated with the Amazon River plume, *Geophys. Res. Lett.*, *30*(24), 2287, doi:10.1029/2003GL018841.
Körtzinger, A. (2010), The outer Amazon plume: An atmospheric CO_2 sink, in *Carbon and Nutrient Fluxes in Continental Margins: A Global Synthesis*, edited by K.-K. Liu et al., pp. 450–453, Springer, New York.
Landschützer, P., N. Gruber, D. C. E. Bakker, and U. Schuster (2014), Recent variability of the global ocean carbon sink, *Global Biogeochem. Cycles*, *28*, 927–949, doi:10.1002/2014GB004853.
Lefèvre, N., D. Diverrès, and F. Gallois (2010), Origin of CO_2 undersaturation in the western tropical Atlantic, *Tellus, Ser. B*, *62*(5), 595–607, doi:10.1111/j.1600-0889.2010.00475.x.
Lefèvre, N., G. Caniaux, S. Janicot, and A. K. Gueye (2013), Increased CO_2 outgassing in February–May 2010 in the tropical Atlantic following the 2009 Pacific El Niño, *J. Geophys. Res. Oceans*, *118*, 1645–1657, doi:10.1002/jgrc.20107.
Lefèvre, N., D. F. Urbano, F. Gallois, and D. Diverrès (2014), Impact of physical processes on the seasonal distribution of the fugacity of CO_2 in the western tropical Atlantic, *J. Geophys. Res. Oceans*, *119*, 646–663, doi:10.1002/2013JC009248.
Mojica Prieto, F. J., and F. J. Millero (2002), The values of pK1 + pK2 for the dissociation of carbonic acid in seawater, *Geochim. Cosmochim. Acta*, *66*(14), 2529–2540, doi:10.1016/S0016-7037(02)00855-4.
Molleri, G. S. F., E. M. L. M. de Novo, and M. Kampel (2010), Space-time variability of the Amazon River plume based on satellite ocean color, *Cont. Shelf Res.*, *30*(3–4), 342–352, doi:10.1016/j.csr.2009.11.015.
O'Reilly, J. E., S. Maritorena, B. G. Mitchell, D. A. Siegel, K. L. Carder, S. A. Garver, M. Kahru, and C. McClain (1998), Ocean color chlorophyll algorithms for SeaWiFS, *J. Geophys. Res.*, *103*(C11), 24,937–24,953, doi:10.1029/98JC02160.
Park, G.-H., and R. Wanninkhof (2012), A large increase of the CO_2 sink in the western tropical North Atlantic from 2002 to 2009, *J. Geophys. Res.*, *117*, C08029, doi:10.1029/2011JC007803.
Pierrot, D., C. Neill, K. Sullivan, R. Castle, R. Wanninkhof, H. Lüger, T. Johannessen, A. Olsen, R. A. Feely, and C. E. Cosca (2009), Recommendations for autonomous underway pCO_2 measuring systems and data-reduction routines, *Deep Sea Res., Part II*, *56*(8–10), 512–522, doi:10.1016/j.dsr2.2008.12.005.
Richey, J. E., J. M. Melack, A. K. Aufdenkampe, V. M. Ballester, and L. L. Hess (2002), Outgassing from Amazonian rivers and wetlands as a large tropical source of atmospheric CO_2, *Nature*, *416*, 617–620, doi:10.1038/416617a.
Rodrigues, R. R., and M. J. McPhaden (2014), Why did the 2011–2012 La Niña cause a severe drought in the Brazilian Northeast?, *Geophys. Res. Lett.*, *41*, 1226–1231, doi:10.1002/2013GL058703.
Sarmiento, J. L. S., and N. Gruber (2006), *Ocean Biogeochemical Dynamics*, 503 pp., Princeton Univ. Press, Princeton, N. J.
Sombroek, W. (2001), Spatial and temporal patterns of Amazon rainfall, *Ambio J. Hum. Environ.*, *30*(7), 388–396, doi:10.1579/0044-7447-30.7.388.
Stramma, L., and F. Schott (1999), The mean flow field of the tropical Atlantic Ocean, *Deep Sea Res., Part II*, *46*(1–2), 279–303, doi:10.1016/S0967-0645(98)00109-X.
Subramaniam, A., et al. (2008), Amazon River enhances diazotrophy and carbon sequestration in the tropical North Atlantic Ocean, *Proc. Natl. Acad. Sci. U.S.A.*, *105*(30), 10,460–10,465, doi:10.1073/pnas.0710279105.
Sweeney, C., E. Gloor, A. R. Jacobson, R. M. Key, G. McKinley, J. L. Sarmiento, and R. Wanninkhof (2007), Constraining global air-sea gas exchange for CO_2 with recent bomb 14C measurements, *Global Biogeochem. Cycles*, *21*, GB2015, doi:10.1029/2006GB002784.
Takahashi, T., J. Olafsson, J. G. Goddard, D. W. Chipman, and S. C. Sutherland (1993), Seasonal variation of CO_2 and nutrients in the high-latitude surface oceans: A comparative study, *Global Biogeochem. Cycles*, *7*(4), 843–878, doi:10.1029/93GB02263.
Takahashi, T., et al. (2009), Climatological mean and decadal change in surface ocean pCO_2, and net sea-air CO_2 flux over the global oceans, *Deep Sea Res., Part II*, *56*(8–10), 554–577, doi:10.1016/j.dsr2.2008.12.009.
Ternon, J. F., C. Oudot, A. Dessier, and D. Diverres (2000), A seasonal tropical sink for atmospheric CO_2 in the Atlantic Ocean: The role of the Amazon River discharge, *Mar. Chem.*, *68*(3), 183–201, doi:10.1016/S0304-4203(99)00077-8.
Weiss, R. F. (1974), Carbon dioxide in water and seawater: The solubility of a non-ideal gas, *Mar. Chem.*, *2*(3), 203–215, doi:10.1016/0304-4203(74)90015-2.
Zhang, D., M. J. McPhaden, and W. E. Johns (2003), Observational evidence for flow between the subtropical and tropical Atlantic: The Atlantic subtropical cells, *J. Phys. Oceanogr.*, *33*(8), 1783–1797, doi:10.1175/2408.1.